Influence of the Transport on the Instability of a Boundary Current

XAVIER J. CAPET

Centre Militaire d'Océanographie, SHOM, Brest, France

LAURENT CHÉRUBIN

Instituto de Oceanografia, faculdade de Cienciâs da Universidad de Lisboa, Portugal

YVES MOREL

Centre Militaire d'Océanographie, SHOM, Brest, France

(Manuscript received 4 October 2001, in final form 8 March 2002)

ABSTRACT

This paper examines the stability properties of coastal currents having the same potential vorticity (PV) structure but different transports and widths. The PV structure is chosen so as to verify the Charney–Stern necessary condition for instability: two PV fronts associated with opposite sign gradients exist. The authors find that the characteristics of the eddies formed by the current are sensitive to the transport and current width, and very different vortex sizes can be obtained when varying the latter parameters. The diameter is indeed shown to diminish when increasing the transport or diminishing the current width. Analytical and numerical results also show that there are parameter ranges for which the current is stable, and that the Charney–Stern criterion is indeed not a sufficient condition for instability. Large transports are, however, necessary to stabilize the current. The model is then used to study the dynamics of a current subject to adiabatic changes, and a few scenarios are reviewed. In particular, the authors explain how eddies with different diameters can be generated from the same current.

1. Introduction

a. Previous work and subject of this study

As underlined by the pioneering work of Charney and Stern (1962), potential vorticity (PV) is a key factor when studying the stability of currents. These authors have indeed shown that, in the framework of the quasigeostrophic (QG) model, a necessary condition for a current to be unstable to barotropic/baroclinic instabilities is that its PV gradient changes sign somewhere in the fluid. Since then, different authors have examined the stability properties of systems in different dynamical regimes (see Griffiths et al. 1982; Ripa 1991; Swaters 1991; Kushner 1995; Benilov 1993, 1994) and have shown that, even in configurations that are far from the QG assumptions, the Charney–Stern (C–S) principle seems still valid (see also in particular Boss et al. 1996).

As the instability of oceanic currents is responsible for the generation of important features (such as meanders and coherent vortices), the sensitivity of their instability properties to different parameters has been the subject of many investigations too. For instance, the influence of boundary conditions and bottom topography have been examined in Mysak et al. (1981); Killworth and Stern (1982) examined the influence of a vertical boundary; Killworth (1983) and Killworth et al. (1984) studied the long-wave instability of a surface front, the effect of the lower layer, and the influence of the stratification; and the vertical shear of the current is studied in Smeed (1988). Pedlosky (1987, chapter 7.15) has considered the effect of horizontal velocity shear on a baroclinically unstable current. Paldor and Ghil (1991) have studied the influence of the total ocean depth and mean current speed, and Bush et al. (1995) the effect of the current symmetry or asymmetry. These papers have underlined the different regimes that can exist when determining parameters are modified. In particular, the most unstable wavelength and size of the eddies that are generated from the current instability can be very sensitive to these parameters. In general, simple models are able to predict the size of the vortices formed by the major oceanic currents, provided the latter are properly chosen. It is, however, interesting to notice that most parameters are linked to the PV of the flow, so

Corresponding author address: Dr. Yves Morel, Nansen Environmental and Remote Sensing Center, Edvard Griegsvei 3A, N-5059 Bergen, Norway.
E-mail: yvesm@nersc.no

changing these parameters also induces a modification of the PV structure. The stabilization of currents for some parameter range sometime observed in the previous studies is thus usually associated with strong transformations of the PV structure where gradients no longer change sign (see, for instance, Pedlosky 1987, chapter 7.15).

Potential vorticity is conserved for each particle as long as the evolution is adiabatic, and is therefore a tracer. Thus, currents transporting a water mass with marked temperature and salinity anomalies have characteristic PV anomalies. The latter should be conserved along the current paths unless diabatic processes are clearly identified and their effect on the PV structure properly evaluated. The influence of mixing on the PV transformation and stability of currents has been examined recently (see Morel and McWilliams 2001), but to our knowledge there only exists few studies evaluating the stability of currents whose structure is changing under adiabatic processes and for which PV is thus fixed.

While the water mass characteristics and PV stay identical, the transport and width of a current can indeed change along its path (for instance the detachment of eddies reduces the transport downstream of the instability) or because of other adiabatic processes associated with seasonal or higher frequency variability. The stability properties or the size of the eddies generated by the current can then be modified. This is the spirit and the main subject of this paper: we study the dynamics of currents with the same PV structure but different transports and widths and analyze the influence of these parameters on the growth rates and most unstable wavelengths.

b. Plan of the study

The configuration and equations we consider in this paper are given in section 2. In section 3, we present and interpret analytical and numerical results and then discuss their application to the ocean (section 4). A summary is given in the last section.

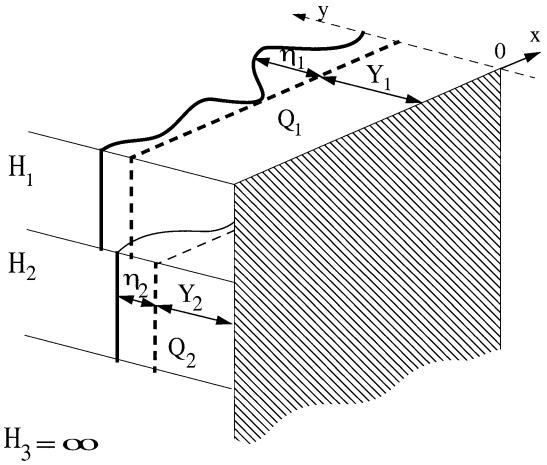

FIG. 1. Model configuration. We consider a 2½-layer model with a piecewise constant PV strip against the eastern boundary in each layer.

2. The configuration and equations

a. Configuration

We consider a model with two active layers overlying an infinitely deep and resting lower layer (see Fig. 1). The upper- and midlayer depths at rest H_1, H_2 and the reduced gravity $g'_{1,2}$, $g'_{2,3}$ of the interfaces between layers 1–2 and 2–3, respectively, are

$$g'_{1,2} = 10^{-2}\ \text{m s}^{-2} \qquad g'_{2,3} = 10^{-2}\ \text{m s}^{-2}$$
$$H_1 = 400\ \text{m} \qquad H_2 = 400\ \text{m}.$$

We also choose a constant Coriolis frequency $f_0 = 10^{-4}$ s^{-1}. These values are fixed for the rest of this study as they are representative of a typical ocean stratification and our general conclusions do not depend on these choices.

The internal radii of deformation associated with this stratification are

$$R_{di}^2 = \frac{2}{(\text{Fr}_1 + \text{Fr}_2 + \text{Fr}_3) + (-1)^i[(\text{Fr}_1 + \text{Fr}_2 + \text{Fr}_3)^2 - 4\text{Fr}_1\text{Fr}_3]^{1/2}},$$

where

$$\text{Fr}_1 = \frac{f_0^2}{g'_{1,2}H_1}, \qquad \text{Fr}_2 = \frac{f_0^2}{g'_{1,2}H_2}, \qquad \text{Fr}_3 = \frac{f_0^2}{g'_{2,3}H_2}$$

are the dimensional Froude numbers. This yields $R_{d1} = 32$ km and $R_{d2} = 12$ km.

The domain is a half plane with a vertical wall at the eastern side. We consider coastal currents intensified near this boundary (located at $y = 0$; see Fig. 1) and associated with uniform PV anomalies in each layer (see Fig. 1). The strength and initial width of these PV strips are (Q_1, Y_1) and (Q_2, Y_2) for layers 1 and 2, respectively.

b. Equations

We restrict our investigations to QG dynamics. Strictly speaking, this assumption constrains the Rossby num-

bers and isopycnal deviations of the currents to be small. When this is not the case, the full shallow-water equations should be used. However, we believe this would only yield quantitative difference and we think most of the physics studied here is retained in the QG model, which permits simpler interpretations. This has been proven in particular by Boss and Paldor (1995) who show that the QG framework is adequate for describing the instability of a PV front even in regimes where the QG assumptions are violated.

It is convenient to nondimensionalize all equations using the first baroclinic radius of deformation $R_{d1} = 32$ km as the horizontal length scale and the inverse PV anomaly in the first layer, $1/|Q_1|$, as the timescale. The nondimensional equations of motion are then (see Pedlosky 1987, chapter 6.16)

$$\partial_t \mathrm{PVA}_k + J(\psi_k, \mathrm{PVA}_k) = 0 \qquad k = 1, 2, \quad (1a)$$

where ψ_k is the streamfunction in layer k, PVA_k is the PV anomaly and is given by

$$\mathrm{PVA}_1 = \nabla^2\Psi_1 + F_1(\Psi_2 - \Psi_1) \quad (1b)$$

$$\mathrm{PVA}_2 = \nabla^2\Psi_2 + F_2(\Psi_1 - \Psi_2) - F_3\Psi_2, \quad (1c)$$

and $J(A, B) = \partial_x A\partial_y B - \partial_x B\partial_y A$ is the Jacobian of A and B; t is the nondimensional time, x and y are the nondimensional coordinates, and $F_i = \mathrm{Fr}_i R_{d1}^2 = 2.6$ ($i = 1, 2, 3$) the nondimensional Froude numbers.

c. Initial state and parameters

As we have chosen piecewise constant PV field, PVA_k can be written

$$\mathrm{PVA}_1 = \begin{cases} 0, & y > Y_1 \\ q_1, & y \le Y_1 \end{cases}$$

$$\mathrm{PVA}_2 = \begin{cases} 0, & y > Y_2 \\ q_2, & y \le Y_2 \end{cases}$$

with $q_1 = Q_1/|Q_1| = \pm 1$ and $q_2 = Q_2/|Q_1|$.

In the appendix, we calculate the initial streamfunction and velocity field associated with the previous general PV anomaly. The calculations show that there exists two degrees of freedom for the velocity field of coastal currents given a PV structure (these corresponds to two Kelvin modes with infinite wavelength and no PV anomaly). These can be chosen so as to determine the velocity field at the coast for instance, but such a parameter is not easy to interpret. In this study, we have chosen to determine the transports within the PV strips of each layer T_1 and T_2. There indeed exists a conservation law for this quantity, which can offer interesting physical interpretations.

In our configuration, as there only exist two PV fronts, q_1 and q_2 must have opposite sign in order to verify the Charney–Stern necessary condition for instability. In the following, to reduce the number of parameters, we chose $q_1 = -q_2 = 1$ and $Y_1 = Y_2 = Y$. We therefore study the sensitivity of the current instability to three parameters: the current width Y, and the transports in each layer, T_1 and T_2.

d. Numerical model

Potential vorticity anomalies can develop near boundaries as a consequence of viscosity (see Morel and McWilliams 2001). Wall friction may be important in laboratory experiments (see Stern and Whitehead 1990) but in nature Reynolds numbers are high and the physical relevance of this phenomenon remains uncertain. It thus seems necessary to minimize this effect in the present study.

Contour dynamics and contour surgery algorithms (Dritschel 1988, 1989) consider piecewise constant PV structures for which the velocity field can be diagnosed from contour integral. Discretizing PV fronts and advecting each nodes with the calculated velocity fields yields a Lagrangian model with adequate PV conservation properties.

The numerical model used in this study is the Contour–Advective Semi Lagrangian (CASL) developed by Drischel and Ambaum (1997). This hybrid algorithm incorporates all aspects of contour surgery, but the PV field is projected on a fine grid and inverted (by finite differences or fast Fourier transforms, depending on the model geometry) to obtain the velocity field. Again this model prevents the development of new PV anomalies.

3. Results

a. Linear instability

In the appendix, we develop an analytical model to calculate the unstable modes and associated growth rates in a general configuration (N layers and as many piecewise constant PV strips as wanted). In our 2½-layer system, Eqs. (A17)–(A18) can be used to study their sensitivity to the transport and current width. In Fig. 2, we plot the maximum growth rate (Fig. 2a) and corresponding wavenumber (Fig. 2b) as a function of the transports in each layer for a fixed current width $Y = 0.75$. In Fig. 3, we plot the maximum growth rate (Fig. 3a) and corresponding wavenumber (Fig. 3b) as a function of the current width and the transport, assuming $T_1 = T_2$.

Figures 2 and 3 show that there exist ranges of transport and width for which the current is stable, which is intriguing as the Charney–Stern necessary condition for instability is verified (there exist opposite sign PV gradients). This underlines that the latter criterion is indeed not sufficient to ensure instability. It is worth noticing that the regions in which the current remains stable are associated with strong transport, preferentially with opposite sign in each layer or small current width.

Another interesting result is the sensitivity of the most

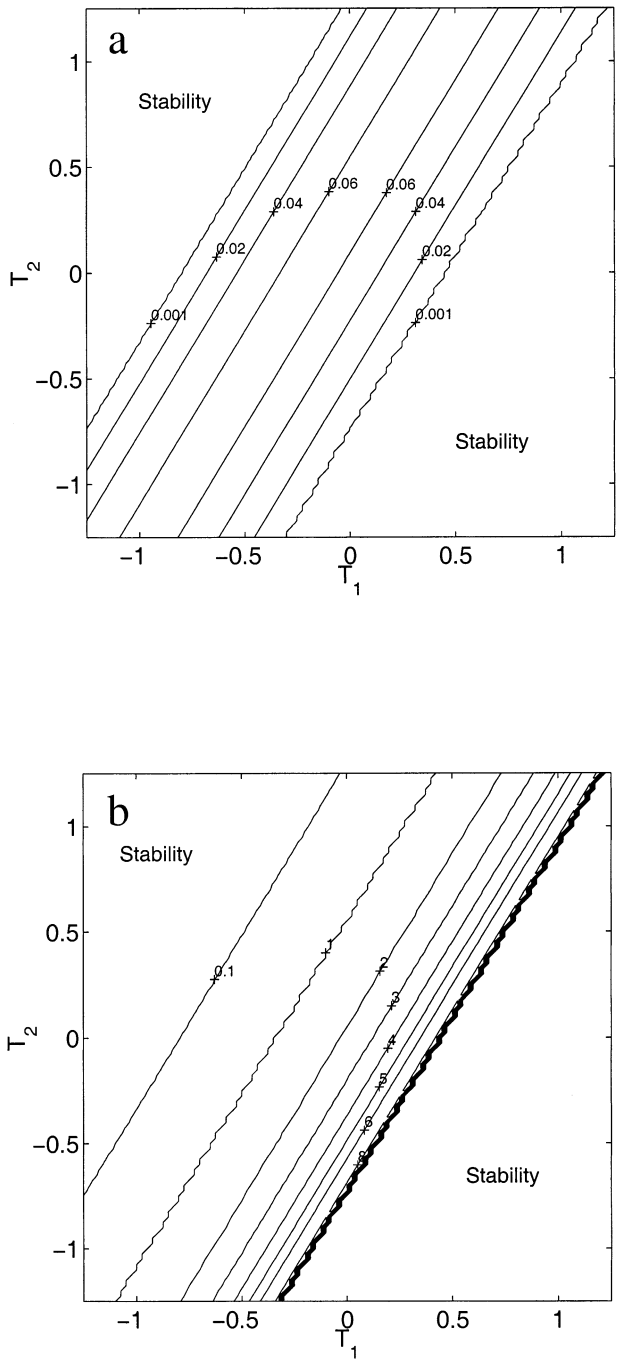

FIG. 2. (a) Maximum growth rate as a function of the transports in each layer T_1 and T_2 (the PV strip width is fixed: $Y_1 = Y_2 = Y = 0.75$), and (b) associated wavenumber k. Notice the stability regions.

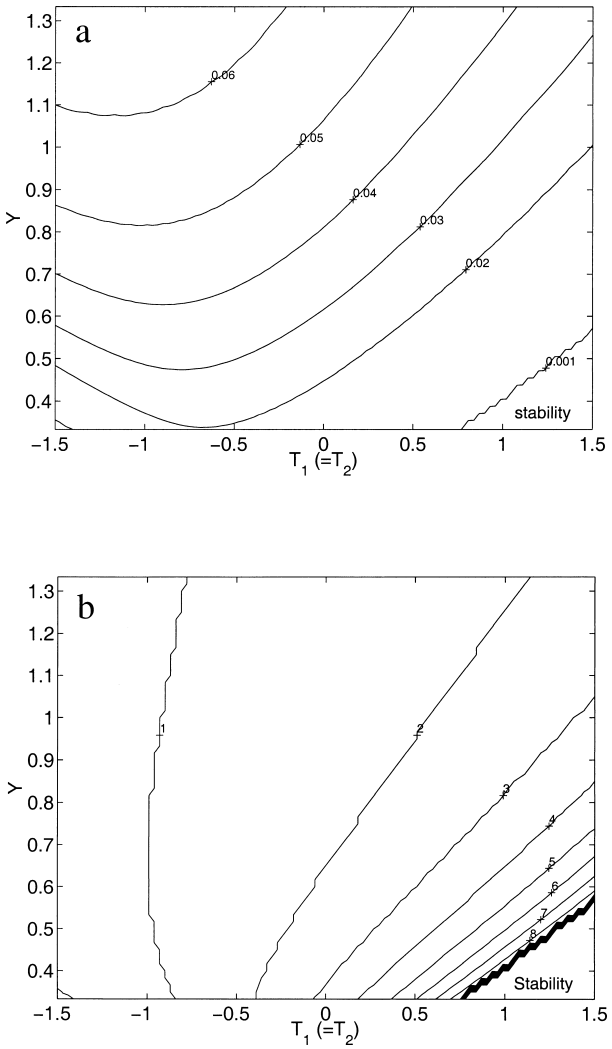

FIG. 3. As in Fig. 2 but (a) as a function of the transport T_1 and PV strip width Y($T_2 = T_1$ here) and (b) associated wavenumber k.

unstable wavenumber (and growth rate) to the transport and current width. Instability gives rise to eddies whose scale are related with the most unstable wavelengths and Figs. 2–3 therefore suggest that the size of the emerging eddies can reach different values provided Y, T_1, and T_2 are properly chosen. Indeed, changing these parameters can lead to the generation of eddies with different characteristics and is illustrated in the next section.

b. Nonlinear evolution

Three experiments, labeled S_1, S_2, and S_3 with different parameter values (see Table 1), are performed to illustrate the previous results. The CASL model of Dritschel and Ambaum (1997) is initialized with the previous configurations. A small white noise perturbation is added to trigger the development of unstable modes.

TABLE 1. Transports in each layer (T, and T_2) and current width (y) for expts S_1, S_2, and S_3.

Expt	T_1	T_2	Y
S_1	0.2	0.2	1.15
S_2	0.6	0.2	1.15
S_3	0.5	0.5	1.15

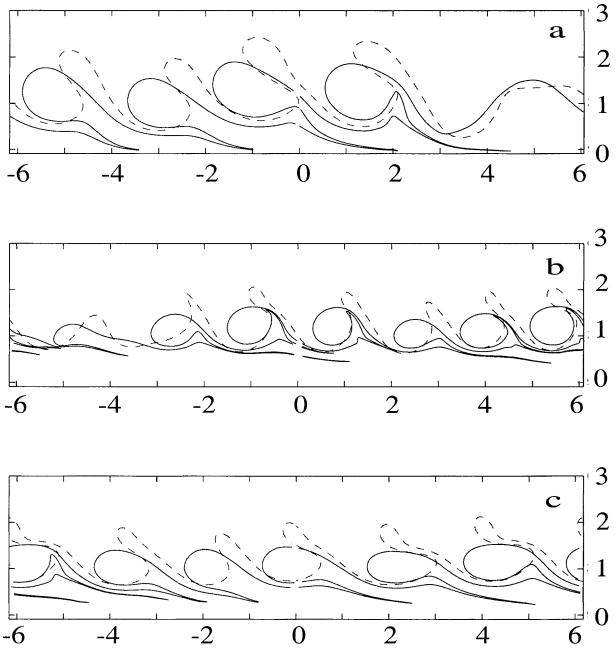

FIG. 4. Potential vorticity fronts in the upper (plain line) and middle (dashed line) layers at $t = 15$ nondimensional time units. Experiments (a) S_1, (b) S_2, and (c) S_3 are represented. Notice the drastic differences in the size of the eddies generated.

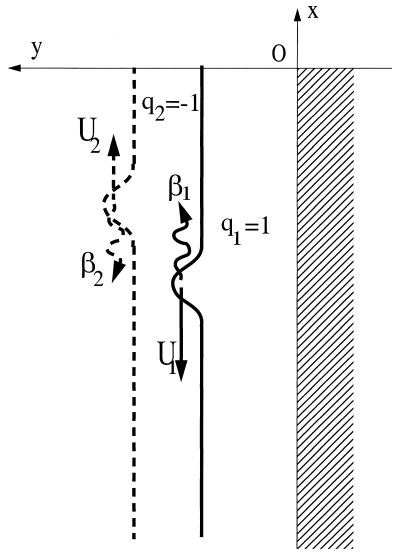

FIG. 5. Schematic diagram of the propagation of perturbations along the PV fronts in layer 1 (plain) and 2 (dashed). The velocity field in the vicinity of each front (U_1 and U_2) induces a displacement that is independent of the perturbation wavelength. On the other hand, the latter is important for the propagation induced by the β-current effect associated with the PV gradients. To interact and reinforce each other, the perturbations in each layer must propagate at the same speed, so that the β-current effect must compensate the shear associated with advection.

Figure 4 represents the PV front in each layer (plain line for the upper layer, dashed one for the middle one) for S_1 (Fig. 4a), S_2 (Fig. 4b), and S_3 (Fig. 4c) and at $t = 15$ nondimensional time units. In all cases, the opposite sign PV fronts interact, forming hetons that detach from the main current. The eddy length scales are very different from an experiment to another as expected from the linear analysis. For instance the radius of the vortices generated in S_1 is about twice that in S_2. Notice the latter is associated with a stronger transport in the upper layer.

c. Interpretation

Different authors have pointed out the physics behind the C–S principle in terms of PV front interaction (see for instance Hoskins et al. 1985; Sakai 1989; Cushman-Roisin 1994, chapters 7 and 16; Pichevin 1998; Morel and McWilliams 2001): when PV fronts associated with opposite sign gradients exist, perturbations can form on each front and interact so as to amplify each other and generate hetons (when the opposite sign PV fronts are located in different layers as in our configuration). As pointed out by Hoskins et al. and Sakai, perturbations along both fronts can only interact and grow if they propagate at the same speed. Conditions are therefore required on their propagation speeds for the instability to develop.

Perturbations propagate as a result of advection and PV gradient effects. The former is associated with the velocity field in the vicinity of the front and is the same for all wavelengths in a layer. When the velocity fields at both PV fronts are different and the current is vertically sheared, advection keeps perturbations from interacting and growing. Obviously, this effect depends on the choice of the transport: the velocity field at a PV front increases (decreases) with the transport in this layer. The PV gradient effect is similar to the planetary β effect on the propagation of Rossby waves and will also be referred to as β-current effect here. As for planetary Rossby waves, it is maximum for long waves (small wavenumbers), decreases toward zero for short waves, and perturbations propagate with high PV values on their right. This effect therefore induces positive propagation speeds in the first layer and negative propagation speeds in the second layer. Thus, wavelengths may exist for which the β-current effect compensates the vertical shear associated with advection so that perturbations can interact as shown for the configurations studied here on Fig. 5. For a given PV gradient, the propagation speed associated with the β-current effect is limited, however. Thus, it cannot compensate the advective effect when the transports become large. This explains the existence of the stability regions in Figs. 2 and 3.

This is underlined in Fig. 6 which represents the velocity profiles for $T_2 = 0.2$ and $Y = 0.75$ and for different values of T_1 ($T_1 = 0.6$, 0.2, -0.2, -0.6, and -0.8). The velocity profile in layer 2 does not vary much for these configurations, and we have only represented the case $T_1 = 0.6$ (thick solid line). The maximum growth rate is given for each configuration. Notice

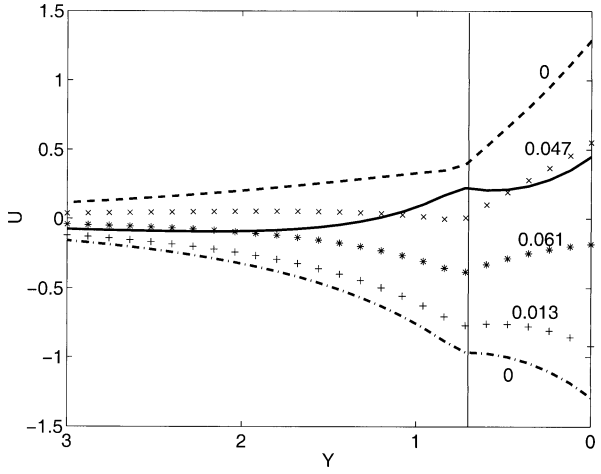

FIG. 6. Velocity profiles for different values of the transport. In all cases, T_2 is set to 0.2 and $Y = 0.75$. The layer-1 velocities are shown for $T_1 = 0.6$ (dashed line), 0.2 (crosses), -0.2 (stars), -0.6 (plus signs), and -0.8 (dash-dotted line). The position of the PV fronts is indicated by the vertical solid line and the maximum growth rate is given for each configuration. The velocity profile in layer-2 weakly vary for these different choices of T_1, and we have only represented the case $T_1 = 0.6$ (thick solid line).

that it is zero for $T_1 = 0.6$ (dashed line on Fig. 6) and $T_1 = -0.8$ (dash-dotted line on Fig. 6), which means that these configuration are stable. As seen above, the difference between the upper- and lower-layer propagation speeds associated with the β-current effect is always positive and can thus only compensate a negative velocity shear. When $T_1 = 0.6$, Fig. 6 shows that the velocity shear is positive and the PV fronts thus cannot interact. When $T_1 = -0.8$, the shear is negative, but its value is large and cannot be compensated by the β-current effect. Again the PV fronts cannot interact and the current becomes stable.

These arguments can also explain the decrease of the generated eddy size when increasing the transport in the previous numerical experiments. Indeed, increasing the transport from 0.2 (S_1) to 0.6 (S_2) in the first layer while keeping the same midlayer transport drastically decreases in absolute value the velocity field difference as a consequence of our relation between streamfunctions and velocities. As a result, weaker β-current-induced propagation speeds are necessary to achieve interaction between both fronts. This is the case for shorter waves that therefore become the most unstable waves. Increasing the transport from 0.2 to 0.5 in both layers leads to the same process: selection of shorter waves and generation of smaller eddies.

4. Discussion

a. Charney–Stern criterion and stability

The Charney–Stern necessary condition for instability often seems sufficient: in most studies, currents with opposite-sign PV gradients are generally unstable to certain wavelengths (see Smeed 1988; Capet and Carton 2002, manuscript submitted to *J. Phys. Oceanogr.*). A few authors, however, noticed the sensitivity of current stability properties to some parameters and that unstable currents can become stable for some regimes.

The influence of the Rossby number on the stability of a coastal current is studied in rotating-tank experiments by Baey (1997). He finds that the current become stable for large Rossby numbers (Ro $\geq$ 1 or so). The coastal currents studied in his experiments are generated by a source of intermediate water and, to achieve large Rossby numbers, the intermediate water flux is increased.

Garnier et al. (1998) use a nonhydrostatic model with very high vertical resolution to examine the evolution of secondary baroclinic instabilities. They analyze the ratio of the local Rossby and Froude numbers (respectively Ro and Fr) and find that instability only develops in regions where Ro/Fr $\leq$ 1.5.

Even though it is delicate to compare our QG model to laboratory experiments with high Rossby numbers or nonhydrostatic simulations, we think Baey (1997) and Garnier et al. (1998) are in agreement with our results, which suggests that currents could become stable when their transport increases above a critical level. In particular, we believe that the stabilizing mechanism is not necessarily associated with ageostrophic effects but, as shown above, with the impossibility of opposite gradient PV fronts to interact when the velocity shear is too strong.

b. Application to the ocean

In our configuration, the transports necessary to obtain stable configurations can be fairly strong and therefore difficult to achieve for oceanic currents. Indeed, for equal transports in each PV strip, Fig. 3 shows that positive transports with $T_1 = T_2 \geq 1$ are necessary when $Y \geq 0.4$. This yields dimensional transports $\hat{T}_i \simeq 1 \times HR_{d1}^2 Q \simeq 4$ Sv (Sv $\equiv 10^6$ m^3 s^{-1}) with $R_{d1} \simeq 30$ km, $H = 400$ m, and a moderate PV anomaly $Q \simeq 0.1 \times 10^{-4}$ s^{-1}. For configurations with opposite sign transports in each layer, smaller transports are necessary (as seen in Fig. 2, the critical nondimensional transports are in the range $|T_i| \simeq 0.5$, which yields $\hat{T}_i \simeq \pm 2$ Sv). These values are reasonable and can be achieved in the ocean, but most coastal currents are associated with much stronger PV anomalies[1] and their critical transport for stability is higher and probably out of reach, at least for currents whose transport is limited.

However, as seen in the previous sections, realistic changes in the characteristics of a current can induces modifications of the eddies it generates. In particular, their horizontal scale can be drastically modified.

In nature, most unstable currents give rise to eddies

[1] The PV anomaly can be estimated from the vorticity of the eddies they generate, which can be calculated from their turnover time.

with different sizes, and our results therefore offer an explanation for this behavior. For instance, the Mediterranean outflow along the Iberian continental slope is unstable and forms eddies (meddies, for Mediterranean Water eddies). Different formation sites exist (see Bower et al. 1997) and the sizes of the generated eddies are highly variable. The smallest meddy ever observed had a diameter[2] $D \simeq 20$ km and was located in the Gulf of Cadiz (Prater and Sanford 1994). Larger meddies with diameter $D \simeq 30$–60 km were observed a few hundred kilometers off the Iberian coast (see Armi et al. 1989; Richardson et al. 1989; Pingree and Le Cann 1993; Tychensky and Carton 1998) or near Cape Finistere (Paillet et al. 1999).

The Mediterranean outflow is also highly variable. Indeed, different authors have observed strong modifications of its maximum velocity or width along its path (see Rhein and Hinrichsen 1993; Baringer 1993; Baringer and Price 1997; Chérubin 2000). Seasonal, and higher-frequency, variability also exists that can lead to important changes in the current structure (Ambar et al. 1999).

After it has mixed with central waters to form an equilibrated middepth current, we can hypothesize that the evolution of the Mediterranean outflow is roughly adiabatic and its PV is conserved. Thus, the existence of eddies with different diameters could be a direct consequence of the modification of the outflow characteristics as predicted by our results. It is, for instance, possible to relate the formation of small eddies in the Gulf of Cadiz to the strong transport that exists in this area. The largest eddies are apparently formed downstream in regions where the transports have decreased, partly as a consequence of meddy generation upstream.

Different interpretations, using different ''paths'' in the *transport*/*width* space are also possible. The modification of these characteristics when an upwelling develops above the Mediterranean outflow could also have drastic consequences on the scale of the eddies generated, which would advocate the influence of seasonal variability. The spreading of the current while keeping the same transport also increases the length scale of the generated eddies (see Fig. 3). Lateral mixing with surrounding waters is likely to widen the current and also increase the nondimensional transport both because of additional waters entrainment and PV dilution. Increasing the current width and the transport have opposite influence so that the effect of lateral mixing is difficult to predict. It, however, modifies the (T, Y) properties of the current and we can expect this process to lead to different eddy scales in general in the ocean.

5. Summary

In this paper, we have examined the different regimes of a coastal current when subject to adiabatic changes. The PV structure is unchanged and is chosen so as to verify the Charney–Stern necessary condition for instability. Other characteristics such as transport and width can, however, be modified, which has drastic consequences on the current dynamics. This is analyzed with an analytical model that calculates the growth rates of unstable waves and with a numerical contour surgery model. In most cases, the current is unstable and generates eddies, but the size of these eddies can be modified when changing the current transport and/or width. Obviously, nonlinear processes also play an important role to determine the scale of the emerging eddies, and this has not been studied here. However, we have shown that different vortex characteristics can be obtained when the transport and current width are modified. In particular, the diameter is shown to diminish when increasing the transport or diminishing the current width.

We have also shown that a critical transport exists above which the current becomes stable, which shows the Charney–Stern criterion is indeed not a sufficient condition for instability. For our stratification our simple PV structure and for coastal currents with strong PV anomalies, we find, however, that the transport necessary to achieve stability is very large, so the Charney–Stern criterion is in practice sufficient for the configuration studied in this paper. The latter result can however not be generalized as it may be sensitive to the PV structures (when $|Q_1| \neq |Q_2|$ or $Y_1 \neq Y_2$, for instance), whose influence has not been explored here.

The physics behind these mechanisms is shown to be related to the interaction of the opposite gradient PV front that exist when the Charney–Stern criterion is verified. Perturbations on both fronts can only interact and lead to meander growth when they propagate at the same speed. Two effects have to be taken into account: advection of the perturbation by the local velocity and self-propagation associated with the PV gradient. The latter depends on the wavelength of the perturbation, which offers a mechanism for scale selection.

Observations often show eddies with various length scales generated from the same current. We then suggest this can be explained by changes in the current characteristics along its path (for instance change in transport due to upstream generation of eddies, or lateral entrainment of surrounding waters) or seasonal or higher frequency variability. Obviously, other explanations are possible. Triggering of some wavelengths by bottom topography or capes (see Chérubin 2000; Pichevin and Nof 1996) or other nonlinear destabilization processes (see, for instance Stern, 1986) can participate in the generation of eddies with various sizes. However, the mechanisms discussed here are likely to play a role for some currents, too.

Acknowledgments. The authors wish to thank David Dritschel for providing his CASL code for the numerical experiments of this study.

[2] The radius and diameter are estimated using the distance of the maximum velocity from the eddy center.

APPENDIX

Initial State and Growth Rate Calculation

a. General case

For the sake of generality we first consider the case of an N-layer system with as many piecewise constant PV strips as wanted in each layer. The potential vorticity anomaly is related to the streamfunction through the general equation

$$\mathbf{PVA} = \nabla^2\mathbf{\Psi} + \mathrm{Fr}\mathbf{\Psi}, \tag{A1}$$

where $\mathbf{PVA} = [\mathrm{PVA}_1, \ldots, \mathrm{PVA}_k, \ldots, \mathrm{PVA}_N]'$, $\mathbf{\Psi} = [\Psi_1, \ldots, \Psi_N]'$, and Fr is an $N \times N$ matrix and is associated with the stretching term. Potential vorticity is assumed piecewise constant, and we can thus write

$$\mathrm{PVA}_k = \sum_j \Delta_{k,j}\mathcal{H}(Y_{k,j} + \eta_{k,j} - y), \tag{A2}$$

where $\mathcal{H}$ is the Heaviside function, $\Delta_{k,j} = Q_{k,j} - Q_{k,j+1}$ is the potential vorticity jump at the jth boundary $y = Y_{k,j} + \eta_{k,j}(x, t)$ separating regions in the kth layer where potential vorticity is respectively $Q_{k,j}$ and $Q_{k,j+1}$, $Y_{k,j}$ is the unperturbed (initial) position of the PV front, and $\eta_{k,j}$ its distortions (see Fig. 1).

As gradients of Q_k give delta functions, Lagrangian conservation of PVA_k yields

$$\frac{D}{Dt}\mathrm{PVA}_k = \sum_j -\Delta_{k,j}\delta(Y_{k,j} + \eta_{k,j} - y)\left(\frac{D}{Dt}y - \frac{D}{Dt}\eta_{k,j}\right) = 0 \qquad k = 1, \ldots, N. \tag{A3}$$

Assuming small perturbations of the initial PV fronts (small η), we can decomposed the current flow into an initial part and a small perturbation,

$$\Phi_k = \overline{\Phi}_k(x) + \Phi'_k(x, y, t) \qquad k = 1, \ldots, N.$$

The initial part of the current $\overline{\Phi}_k$ verifies for each layer k

$$\nabla^2\overline{\Phi}_k + \mathrm{Fr}\overline{\mathbf{\Phi}}|_k = \frac{d^2\overline{\Phi}_k}{dy^2} + \mathrm{Fr}\overline{\mathbf{\Phi}}|_k = \sum_j \Delta_{k,j}\mathcal{H}(Y_{k,j} - y) \qquad k = 1, \ldots, N, \tag{A4}$$

while Φ'_k then satisfies the equation

$$\nabla^2\Phi'_k + \mathrm{Fr}\mathbf{\Phi}'|_k = \sum_j \Delta_{k,j}[\mathcal{H}(Y_{k,j} + \eta_{k,j} - y) - \mathcal{H}(Y_{k,j} - y)] \qquad k = 1, \ldots, N,$$

which gives at leading order in the small η limit

$$\nabla^2\Phi'_k + \mathrm{Fr}\mathbf{\Phi}'|_k = \sum_j \Delta_{k,j}\eta_{k,j}\delta(Y_{k,j} - y). \tag{A5}$$

Equation (A3) can then be linearized and we get

$$\frac{\partial}{\partial t}\eta_{k,j} + \overline{U}_{k,j}\frac{\partial}{\partial x}\eta_{k,j} = V_{|Y_{k,j}}, \tag{A6}$$

where $\overline{U}_{k,j} = -d\overline{\Phi}_k/dy(Y_{k,j})$ is the alongshore initial velocity field and $V_{|Y_{k,j}} = \partial_x\Phi'(x, Y_{k,j}, t)$ is the cross-shore velocity associated with the perturbation of the PV front. Here $\overline{U}_k$ can be calculated by differentiating Eq. (A4),

$$\frac{d^2\overline{U}_k}{dy^2} + \mathrm{Fr}\overline{\mathbf{U}}|_k = \sum_j \Delta_{k,j}\delta(Y_{k,j} - y), \tag{A7}$$

and V_k can be calculated assuming $\eta_{k,j} = \eta_{k,j}\exp(lx - \omega t)$ and $\Phi'_k = \Phi'_k(y)\exp(lx - \omega t)$, which yields for Eq. (A5)

$$\frac{d^2\Phi'_k}{dy^2} + (\mathrm{Fr} - l^2Id)\mathbf{\Phi}'|_k = \sum_{k,j} \Delta_{k,j}\eta_{k,j}\delta(Y_{k,j} - y). \tag{A8}$$

Notice that the latter equation is subject to a closed boundary condition at the eastern boundary

$$\Phi'_k(y = 0) = 0, \tag{A9}$$

while Eq. (A7) is not.

Equations (A7) and (A8) are similar and their general form can be written

$$\nabla_l^2\varphi_k + \mathrm{Fr}\boldsymbol{\varphi}|_k = \Gamma_k \tag{A10}$$

with

$$\nabla_l^2 = \partial_{y^2} - l^2.$$

This equation can be solved in terms of the vertical eigenmodes $P^{(n)} = [P_1^{(n)}, \ldots, P_k^{(n)}, \ldots, P_N^{(n)}]$ associated with the vortex-stretching matrix Fr, so

$$\mathrm{Fr}P^{(n)} = -\gamma_n^2P^{(n)},$$

where $-\gamma_n^2$ is the corresponding eigenvalue. We also define the matrix α, inverse of matrix P whose column are the eigenvectors $P^{(n)}$, with coefficients $\alpha_k^{(n)}$ defined by $\Sigma_n\,\alpha_k^{(n)}P_m^{(n)} = \delta_{km}$. Thus, if we set

$$\varphi_k = \sum_n \varphi^{(n)}P_k^{(n)} \qquad \Gamma_k = \sum_n P_k^{(n)}\Gamma^{(n)}$$

$$\Gamma^{(n)} = \sum_m \alpha_m^{(n)}\Gamma_m,$$

$\varphi^{(n)}$ verifies

$$\nabla_l^2\varphi^{(n)} - \gamma_n^2\varphi^{(n)} = \Gamma^{(n)}. \tag{A11}$$

A Green's function $G_l^{(n)}(y|y')$ for the operator of the left-hand side [when $\Gamma^{(n)} = \delta(y - y')$] is given by

$$G_l^{(n)}(y|y') = \begin{cases} -\dfrac{\exp(-\gamma_n^l y)}{\gamma_n^l}\sinh(\gamma_n^l y'), & y > y' \\ -\dfrac{\exp(-\gamma_n^l y')}{\gamma_n^l}\sinh(\gamma_n^l y), & y < y' \end{cases} \tag{A12}$$

with $\gamma_n^l = \sqrt{\gamma_n^2 + l^2}$. In the rigid-lid approximation and for the flat-bottom case, there exists a barotropic mode associated with $\gamma_0 = 0$ so that for $l = 0$ (A12) becomes

$$G_0^{(0)}(y|y') = \begin{cases} -y' & y > y' \\ -y & y < y'. \end{cases} \quad \text{(A13)}$$

The general solution of (A11) is thus

$$\varphi^{(n)}(y) = \int G_l^{(n)}(y|y')\Gamma^{(n)}(y')\,dy' + A^{(n)}\exp(\gamma_n y) + B^{(n)}\exp(-\gamma_n y),$$

so the general solution of (A10) is given by

$$\varphi_k(y) = \sum_{n,m} P_k^{(n)}\alpha_m^{(n)} \int G_l^{(n)}(y|y')\Gamma_m(y')\,dy' + \sum_n P_k^{(n)}[A^{(n)}\exp(\gamma_n y) + B^{(n)}\exp(-\gamma_n y)]. \quad \text{(A14)}$$

Using Eq. (A13) and the boundary conditions (A9), we can then solve Eqs. (A7)–(A8) with the previous general solutions, and we get

$$\overline{U}_k = \sum_{n,m,i} P_k^{(n)}\alpha_m^{(n)}\Delta_{m,i}G_0^{(n)}(y|Y_{m,i}) + \sum_n P_k^{(n)}[A^{(n)}\exp(\gamma_n y) + B^{(n)}\exp(-\gamma_n y)] \quad \text{(A15)}$$

$$\Phi_k'(y) = -\sum_{n,m,i} P_k^{(n)}\alpha_m^{(n)}\Delta_{m,i}\eta_{m,i}G_l^{(n)}(y|Y_{m,i}). \quad \text{(A16)}$$

Notice that the coefficients $A^{(n)}$ and $B^{(n)}$ are degrees of freedom for the initial state. Finite velocity at $y = +\infty$, however, imposes $A^{(n)} = 0$, but $B^{(n)}$ can be calculated so as to choose the velocity field at the coast, for instance, or any other chosen constraint.

Equations (A6) and (A15)–(A16) then yield

$$\sum_{m,i} A_{k,j;m,i}\eta_{m,i} = \frac{\omega}{l}\eta_{k,j}, \quad \text{(A17)}$$

where

$$A_{k,j;m,i} = \overline{U}_k(Y_{k,j})\delta_{km}\delta_{ij} - \sum_n P_k^{(n)}\alpha_m^{(n)}\Delta_{m,i}G_l^{(n)}(Y_{k,j}|Y_{m,i}). \quad \text{(A18)}$$

The growth rates of the unstable wavenumbers l are then given by the imaginary part of the eigenvalues of matrix **A**.

b. Present configuration

The previous calculation can then be used to calculate the growth rates in the 2½-layer configuration with a single PV front in each layer. The Froude matrix Fr is given by

$$\mathrm{Fr} = \begin{pmatrix} -F_1 & F_1 \\ F_2 & -F_2 - F_3 \end{pmatrix}, \quad \text{(A19)}$$

whose eigenvalues are

$$\gamma_1^2 = \frac{F_1 + F_2 + F_3 + \sqrt{(F_1 + F_2 + F_3)^2 - 4F_1F_3}}{2}$$

$$\gamma_2^2 = \frac{F_1 + F_2 + F_3 - \sqrt{(F_1 + F_2 + F_3)^2 - 4F_1F_3}}{2}.$$

The matrix P containing the eigenmodes $P^{(1)}$ and $P^{(2)}$ is given by

$$P = \begin{pmatrix} P_1^{(1)} & P_1^{(2)} \\ P_2^{(1)} & P_2^{(2)} \end{pmatrix} = \begin{pmatrix} F_1 & F_1 \\ F_1 - \gamma_2^2 & F_1 - \gamma_1^2 \end{pmatrix} \quad \text{(A20)}$$

and its inverse α by

$$\alpha = P^{-1} = \begin{bmatrix} \alpha_1^{(1)} & \alpha_1^{(2)} \\ \alpha_2^{(1)} & \alpha_2^{(2)} \end{bmatrix} = \frac{1}{F_1(\gamma_2^2 - \gamma_1^2)}\begin{pmatrix} F_1 - \gamma_1^2 & -F_1 \\ F_1 + \gamma_2^2 & F_1 \end{pmatrix}. \quad \text{(A21)}$$

The free coefficients $B^{(1)}$ and $B^{(2)}$ are chosen so that

$$\int_0^Y \overline{U}_k\,dy = T_k,$$

where $\overline{U}_k$ is given by Eq. (A15). Notice that, in the present configuration, there only exist two PV fronts, one in each layer, with identical width, so that $Y_{k,j} = Y$ here.

As there only exists a single PV front in each layer, **A** is a 2×2 matrix whose coefficients are given by

$$A_{1,1} = \overline{U}_1(Y) - \sum_n P_1^{(n)}\alpha_1^{(n)}Q_1G_l^{(n)}(Y|Y)$$

$$A_{1,2} = -\sum_n P_1^{(n)}\alpha_2^{(n)}Q_2G_l^{(n)}(Y|Y)$$

$$A_{2,1} = -\sum_n P_2^{(n)}\alpha_1^{(n)}Q_1G_l^{(n)}(Y|Y)$$

$$A_{2,2} = \overline{U}_2(Y) - \sum_n P_2^{(n)}\alpha_2^{(n)}Q_2G_l^{(n)}(Y|Y)$$

with

$$G_l^{(n)}(Y|Y) = -\frac{\exp(-\gamma_n^l Y)}{\gamma_n^l}\sinh(\gamma_n^l Y). \quad \text{(A22)}$$

REFERENCES

Ambar, I., L. Armi, A. Bower, and T. Ferreira, 1999: Some aspects of time variability of the Mediterranean water off South Portugal. *Deep-Sea Res.,* **46A,** 1109–1136.

Armi, L., D. Hebert, N. Oakey, J. F. Price, P. L. Richardson, H. T. Rossby, and B. Ruddick, 1989: Two years in the life of a Mediterranean salt lens. *J. Phys. Oceanogr.,* **19,** 354–370.

Baey, J. M., 1997: Instabilités d'un courant d'eau intermédiaire. Ph.D. thesis, University Joseph Fourier, Grenoble, France, 201 pp.

Baringer, M. O., 1993: Mixing and dynamics of the Mediterranean outflow. Ph.D. thesis, Massachusetts Institute of Technology/Woods Hole Oceanographic Institution Joint Program in Oceanography, WHOI-93-52, 244 pp. [Available from Woods Hole Oceanographic Institute, Woods Hole, MA 02543.]

——, and J. Price, 1997: Mixing and spreading of the Mediterranean outflow. *J. Phys. Oceanogr.,* **27,** 1654–1677.

Benilov, E. S., 1993: Baroclinic instability of large-amplitude geostrophic flows. *J. Fluid Mech.,* **251,** 501–514.

——, 1994: Dynamics of large-amplitude geostrophic flows: The case of strong beta-effect. *J. Fluid Mech.,* **262,** 157–169.

Boss, E., N. Paldor, and L. Thompson, 1996: Stability of a potential vorticity front from quasi-geostrophy to shallow water. *J. Fluid. Mech.,* **315,** 65–84.

Bower, A. S., L. Armi, and I. Ambar, 1997: Lagrangian observations of meddy formation during a Mediterranean undercurrent seeding experiment. *J. Phys. Oceanogr.,* **27,** 2545–2575.

Bush, A. B. G., J. C. McWilliams, and W. R. Peltier, 1995: The formation of oceanic eddies in symmetric and asymmetric jets. Part I: Early time evolution and bulk eddy transport. *J. Phys. Oceanogr.,* **25,** 1959–1979.

Charney, J. G., and M. E. Stern, 1962: On the instability of internal baroclinic jets in a rotating atmosphere. *J. Atmos. Sci.,* **19,** 159–172.

Chérubin, L., 2000: Descriptive analysis of the hydrology and mixing of the Mediterranean outflow and effects of topography on the stability of the Mediterranean undercurrents. Ph.D. thesis, Université de la Méditerranée, Centre d'Océanologie de Marseille, 343 pp.

Cushman-Roisin, B., 1994: *Introduction to Geophysical Fluid Dynamics.* Prentice-Hall, 320 pp.

Dritschel, D. G., 1988: Contour surgery: A topological reconnection scheme for extended integrations using contour dynamics. *J. Comput. Phys.,* **77,** 240–266.

——, 1989: Contour dynamics and contour surgery: Numerical algorythms for extended, high-resolution modelling of vortex dynamics in two dimensional, inviscid, incompressible flows. *Comput. Phys. Rep.,* **10,** 77–146.

——, and M. H. P. Ambaum, 1997: A contour-advective semi-Lagrangian numerical algorithm for simulating fine-scale conservative dynamical fields. *Quart. J. Roy. Meteor. Soc.*, **123,** 1097–1130.

Garnier, E., O. Métais, and M. Lesieur, 1998: Synoptic and frontal-cyclone scale instabilities in baroclinic jet flows. *J. Atmos. Sci.,* **55,** 1316–1335.

Griffiths, R. W., P. D. Killworth, and M. E. Stern, 1982: Ageostrophic instability of ocean currents. *J. Fluid Mech.,* **117,** 343–377.

Hoskins, B. J., M. E. McIntyre, and A. W. Robertson, 1985: On the use and significance of isentropic vorticity maps. *Quart. J. Roy. Meteor. Soc.,* **111,** 877–946.

Killworth, P. D., 1983: Long-wave instability of an isolated front. *Geophys. Astrophys. Fluid Dyn.,* **25,** 235–258.

——, and M. E. Stern, 1982: Instabilities on density-driven boundary currents and fronts. *Geophys. Astrophys. Fluid Dyn.,* **22,** 1–28.

——, N. Paldor, and M. E. Stern, 1984: Wave propagation and growth on a surface front in a two-layer geostrophic current. *J. Mar. Res.,* **42,** 761–785.

Kushner, P., 1995: A generalized Charney–Stern theorem for the semi-geostrophic dynamics. *Tellus,* **47,** 541–547.

Morel, Y., and J. McWilliams, 2001: Effects of isopycnal and diapycnal mixing on the stability of oceanic currents. *J. Phys. Oceanogr.,* **31,** 2280–2296.

Mysak, L. A., E. R. Johnson, and W. W. Hsieh, 1981: Baroclinic and barotropic instabilities of coastal currents. *J. Phys. Oceanogr.,* **11,** 209–230.

Paillet, J., B. Le Cann, A. Serpette, Y. Morel, and X. Carton, 1999: Real-time tracking of a Galician meddy. *Geophys. Res. Lett.,* **26,** 1877–1880.

Paldor, N., and M. Ghil, 1991: Shortwave instabilities of coastal currents. *Geophys. Astrophys. Fluid Dyn.,* **58,** 225–241.

Pedlosky, J., 1987: *Geophysical Fluid Dynamics.* 2d ed. Springer-Verlag, 710 pp.

Pichevin, T., 1998: Baroclinic instability in a three layer flow: A wave approach. *Dyn. Atmos. Oceans,* **28,** 179–204.

——, and D. Nof, 1996: The eddy canon. *Deep-Sea Res.,* **43,** 1475–1507.

Pingree, R. D., and B. Le Cann, 1993: Structure of a meddy (Bobby 92) southeast of the Azores. *Deep-Sea Res.,* **40,** 2077–2103.

Prater, M., and T. Sanford, 1994: A meddy off Cape St. Vincent. Part I: Description. *J. Phys. Oceanogr.,* **24,** 1572–1586.

Rhein, M., and H. Hinrichsen, 1993: Modification of the Mediterranean water in the Gulf of Cadiz, studied with hydrographic, nutrient and chlorofluoromethane. *Deep-Sea Res.,* **40,** 267–291.

Richardson, P. L., D. Walsh, L. Armi, M. Schroder, and J. F. Price, 1989: Tracking three meddies with SOFAR floats. *J. Phys. Oceanogr.,* **19,** 371–383.

Ripa, P., 1991: General stability conditions for a multi-layer model. *J. Fluid Mech.,* **222,** 119–137.

Sakai, S., 1989: Rossby–Kelvin instability: A new type of ageostrophic instability caused by a resonance between Rossby waves and gravity waves. *J. Fluid Mech.,* **202,** 149–175.

Smeed, D. A., 1988: Baroclinic instability of three-layer flows. Part 1: Linear stability. *J. Fluid Mech.,* **194,** 217–231.

Stern, M. E., 1986: On the amplification of convergences in coastal currents and the formation of ''squirts.'' *J. Mar. Res.,* **44,** 403–421.

——, and J. A. Whitehead, 1990: Separation of boundary jet in a rotating fluid. *J. Fluid Mech.,* **217,** 41–69.

Swaters, G. E., 1991: On the baroclinic instability of cold-core coupled density fronts on a sloping continental shelf. *J. Fluid Mech.,* **224,** 361–382.

Tychesky, A., and X. Carton, 1998: Hydrological and dynamical characterization of meddies in the Azores region: A paradigm for baroclinic vortex dynamics. *J. Geophys. Res.,* **103C,** 25 061–25 079.